Turkish Journal of Electrical Engineering & Computer Sciences

http://journals.tubitak.gov.tr/elektrik/

Research Article

Turk J Elec Eng & Comp Sci
(2017) 25: 2943 – 2955

doi:10.3906/elk-1606-260

Multiphase segmentation based on new signed pressure force functions and one level set function

Haider ALI[1], **Noor BADSHAH**[2,*], **Ke CHEN**[3], **Gulzar Ali KHAN**[1], **Nosheen ZIKRIA**[1]
[1]Department of Mathematics, University of Peshawar, Peshawar, Pakistan
[2]Department of Basic Sciences, UET Peshawar, Peshawar, Pakistan
[3]Department of Mathematical Sciences, University of Liverpool, Liverpool, UK

Received: 15.06.2016 • **Accepted/Published Online:** 11.11.2016 • **Final Version:** 30.07.2017

Abstract: In this paper we propose a new model to detect multiple objects of various intensities in images having maximum, minimum, or middle-intensity background by evolving only one level set function. In this model, a new signed pressure force function based on novel generalized averages is used for segmentation of images with maximum or minimum intensity background. For images with middle-intensity backgrounds, which are indeed challenging for 2-phase models, we propose a new product generalized signed pressure force function. Finally, to give experimental and qualitative evidence, our model is tested on both synthetic and real images with the Jaccard similarity index. The experimental and qualitative results reveal that the proposed method is efficient in both global and selective segmentation. Our new model is also tested on color images and the results are compared with the state-of-the-art models.

Key words: Segmentation, level set, geodesic active contours, spf function

1. Introduction

Image segmentation aims to extract or distinguish objects from each other in images. In simple words, image segmentation extracts objects by distinguishing the foreground and background in images [1–6]. Variational image segmentation models are categorized into two classes, namely edge-based models and region-based models. In edge-based models objects are extracted by capturing their boundaries, while in region-based models objects are detected by detecting their occupied optimal regions. For edge detection most of the models use an edge detector function, which mainly depends on the gradient of a given image [4,7,8]. On the other hand, region-based segmentation models use region detectors, known as fidelity terms, which use image statistical information to capture objects/regions [9–11]. In region-based models one of the famous models is the Mumford–Shah (MS) model [10], which is given by:

$$F(u,K)^{MS} = \int_{\Omega} (u-u_0)^2 dxdy + \alpha^* \int_{\Omega - K} |\nabla u|^2 dxdy + \beta \int_K ds, \tag{1}$$

where u_0 is the given image, u is the required solution and is a smooth approximation of u_0, $\alpha^*, \beta > 0, \Omega$ is the image domain, and K is the set of edges (discontinuities) in the image. This model is theoretically very strong but computationally very complex. The first variation of this model is the piecewise constant MS model, which considers u to be piecewise constant in each region. The level set methods [12] provided a

*Correspondence: noor2knoor@gmail.com

good numerical implementation of piecewise constant (PC) MS models [5,13], but unfortunately for multiregion image segmentation multilevel set functions are usually evolved, which is a time-consuming approach in many situations. To enhance the performance of the PC model, Li et al. [9] proposed the local binary fitting model by incorporating the image local statistical information in the PC model [5,14,15]. This model may segment images with intensity inhomogeneity and gives competing results compared to the state-of-the-art models. In this model Gaussian kernel functions are used instead of average intensities. This model works well for images having intensity inhomogeneity, but the computational cost is very high [16]. To overcome this drawback, Wang et al. proposed a local energy-based model (local Chan–Vese (LCV)), [15] which is given by:

$$\begin{aligned} F(\phi, c_1, c_2, d_1, d_2)^{LCV} &= \mu \int_{\Omega} |\nabla H(\phi)| \, dxdy + \lambda_1 \int_{\Omega} \left((u_0 - c_1)^2 + (u_0^* - u_0 - d_1)^2\right) H(\phi) dxdy \\ &\quad + \lambda_2 \int_{\Omega} \left((u_0 - c_2)^2 + (u_0^* - u_0 - d_2)^2\right) (1 - H(\phi)) \, dxdy, \quad (2) \end{aligned} \tag{2}$$

where u_0^* denotes the smooth version of given image u_0 [15]. μ, λ_1, $\lambda_2 > 0$ are trade-off parameters and c_1, c_2, d_1, d_2 are average intensities of the given image and difference image inside and outside the level set function ϕ, respectively. $H(\phi)$ is the Heaviside function, which is 0 if $\phi < 0$ and 1 if $\phi > 0$. Similarly, Zhang et al. proposed an active contour model based on local image fitting [16] for images with intensity inhomogeneity. Recently, Zhang et al. [16–18] combined the idea of geodesics [4] and the Chan–Vese [5] model and proposed the geodesic-aided Chan–Vese (GCV) model as follows:

$$\begin{aligned} &\tfrac{\partial \varphi}{\partial t} = \alpha(spf). \left|\nabla \varphi\right|, \ in \ \Omega, \\ &\varphi\left(t, x, y\right) = \varphi_0\left(x, y\right), \ in \ \Omega, \end{aligned} \tag{3}$$

where spf denotes the signed pressure force function [16–18] and $\alpha > 0$. Similarly, Akram et al. [1] modified the model in Eq. (3) for images with intensity inhomogeneity by replacing the spf function with their local-spf function [1]. Although these models have improved the performance of the region-based active contour models, they are not designed to handle images having multiple intensity objects [16,17]. For quantitative comparison we will use the Jaccard similarity (JS) for different models. If we denote the segmented region by R_1 and the ground truth (GT) by R_2, the JS is the ratio of the areas of the intersection by the union of the regions, i.e. $JS(R_1, R_2) = \frac{|R_1 \cap R_2|}{|R_1 \cup R_2|}$. For better results we want JS to be close to 1. The GT used in this paper is obtained manually in the following way: based on the maximum intensity we set a threshold value and then we choose GT as image $\leq$ threshold value. In the hardware image, the intensity values of all objects are at the most 230; we choose threshold value 240 and take GT as image ≤ 240.

In this paper, we will propose models to handle the problems discussed above. Our novel model uses a single level set function for segmentation of multiregion images having backgrounds of either maximum intensity, minimum intensity, or average intensity and the objects are of homogeneous intensities. The new model is tested on both synthetic and real images. Moreover, some tests on color images are also conducted and results are compared with a standard model.

Furthermore, for quantitative comparison of different segmentation models, the JS index [13] is presented. From experimental results, it can be seen that our proposed model perform better than the state-of-the-art models. It can also be seen that our proposed model works equally well in both global and selective segmentation.

The rest of paper is organized in the following way. In the next section some important materials and

methods are discussed and the proposed model is given. In Section 3 experimental results and discussions about the experiments are given. In Section 4 conclusions are given.

2. The proposed model for multiregion segmentation

In the 2-phase framework, the averages of the Chan–Vese (CV) model [5] consider objects of high intensities as background and objects with low intensities as foreground, so the CV and GCV models are only capable of detecting objects of either high or lower intensities. To handle this type of issue we design a new model based on generalized averages, which is defined in the next section. In images with maximum intensity background, we need larger values of generalized averages than the CV averages to detect all the objects. Similarly, in images with minimum intensity background, we need smaller values of generalized averages than the CV averages to detect all the objects.

2.1. Generalized averages in the segmentation framework

Definition 1 *We define generalized averages in the following way:*

$$G_{c_1} = \frac{\int\limits_{\Omega} u_0^{\beta} H(\varphi)\, dxdy}{\int\limits_{\Omega} u_0^{\beta-1} H(\varphi)\, dxdy}, G_{c_2} = \frac{\int\limits_{\Omega} u_0^{\beta} (1 - H(\varphi))\, dxdy}{\int\limits_{\Omega} u_0^{\beta-1} (1 - H(\varphi))\, dxdy}, \tag{4}$$

where β is any real number, u_0 is the given image, and H is the Heaviside function whose value is 0 if $\phi < 0$ and 1 if $\phi > 0$. The above family of averages is called the Av-family.

Remark 1 *The value of parameter β should be chosen greater than 1 for images of maximum intensity background, like $\beta = 2$. For images of minimum intensity background the value of parameter β should be chosen smaller than 1, such as $\beta = -2$. For images of middle-intensity background, it has been observed that β and the number of pixels carrying maximum intensity are proportional. Experimentally we have derived the following relation, where 0.03 is the average of ratios of β to number of pixels carrying maximum intensity:*

$$\beta = 0.03 \times number\ of\ pixels\ carrying\ maximum\ intensity$$

Now we consider the generalized averages in discrete form as

$$G_{average} = \frac{\sum\limits_{(i,j)} u_0(i,j)^{\beta}}{\sum\limits_{(i,j)} u_0(i,j)^{\beta-1}}. \tag{5}$$

Let us consider the following theorem for analysis.

Theorem 1 *For any positive real numbers $x_1, x_2, ..., x_n$, then*

(I) $\lim\limits_{\beta \to \infty} G_{average} = Max\{x_1, x_2, ..., x_n\}$,

(II) $\lim\limits_{\beta \to -\infty} G_{average} = Min\{x_1, x_2, ..., x_n\}$.

Proof Let us suppose that $x_1 \geq x_2 \geq, ..., \geq x_n$ (which is possible by relabeling and combining terms together). Then $\lim_{\beta\to\infty} G_{average}(x_1, x_2, ..., x_n) = \lim_{\beta\to\infty} \frac{\sum_{i=1}^{n} x_i^{\beta}}{\sum_{i=1}^{n} x_i^{\beta-1}} = \lim_{\beta\to\infty} \frac{x_1^{\beta} \sum_{i=1}^{n} \left(\frac{x_i}{x_1}\right)^{\beta}}{x_1^{\beta-1} \sum_{i=1}^{n} \left(\frac{x_i}{x_1}\right)^{\beta-1}} = x_1 = Max\{x_1, x_2, ..., x_n\}$. Next, to prove the second part, we proceed as follows:

$$\lim_{\beta\to-\infty} G_{average} = \lim_{\beta\to-\infty} \frac{\sum_{i=1}^{n} x_i^{\beta}}{\sum_{i=1}^{n} x_i^{\beta-1}} = \lim_{\beta\to-\infty} \frac{x_n^{\beta} \sum_{i=1}^{n} \left(\frac{x_i}{x_n}\right)^{\beta}}{x_n^{\beta-1} \sum_{i=1}^{n} \left(\frac{x_i}{x_n}\right)^{\beta-1}} = x_n = Min\{x_1, x_2, ..., x_n\}.$$

This result validates that the more β deviates from 1 in a positive direction, i.e. $\beta = 2,\ 3,\ 4,\ 5, ...$, the averages deviate from the central value and tend towards the maximum value of their respective data set. Similarly, the more β deviates from 1 in a negative direction, i.e. $\beta = 0,\ -1,\ -2,\ -3, ...$, the averages deviate from the central value and tend towards the minimum value of their respective data set. Thus, we now have Eq. (2), which can provide averages according to the images. □

Remark 2 *Although $G_{average}$ finds minimum and maximum value as $\beta \to -\infty$, and $\beta \to \infty$ respectively is shown mathematically in double precision, this is not the case for numerical overflows. This is given in Figures 1a and 1b by taking a set of ten numbers $3, 5, 7, \ldots, 21\}$ and $G_{average}$ is plotted against β.*

2.2. Segmenting images with minimum or maximum intensity background

In this subsection we design a new formulation based on the spf function with generalized averages to segment images having minimum or maximum intensity background. For this, we define a novel generalized spf function based on generalized averages as follows:

Definition 2 *The generalized spf function, denoted by Gspf, is defined as follows:*

$$Gspf_{\beta}(u_0) = \frac{u_0(x,y) - \frac{G_{c_1}+G_{c2}}{2}}{\max\left(\left|u_0(x,y) - \frac{G_{c_1}+G_{c2}}{2}\right|\right)}, \text{ where } (x,y) \in \Omega. \tag{6}$$

In particular, for $\beta = 1$, we have averages of the CV model [6] and consequently we have the spf function of [18]. The quality of detection in spf-based models is totally dependent on signs of an spf function and the 2-phase homogeneous case is simple and can be seen in [18]. For complete detection of the foreground and background in an image, the Gspf function must have opposite signs in the foreground and background; otherwise, the result will be incomplete. The signs of the Gspf function depend on the values of averages, which are clear from Eq. (2), and we validate from the following tests that the types of averages that we use influence the quality of detection. Figures 1c–1f illustrate that for different values of parameter β we have different values of averages, which help in capturing all multiple-intensity objects in an image. The given image in this case is a maximum background image and the increment in β causes the detection of all the objects. Now we give some theoretical results for justification of the proposed model.

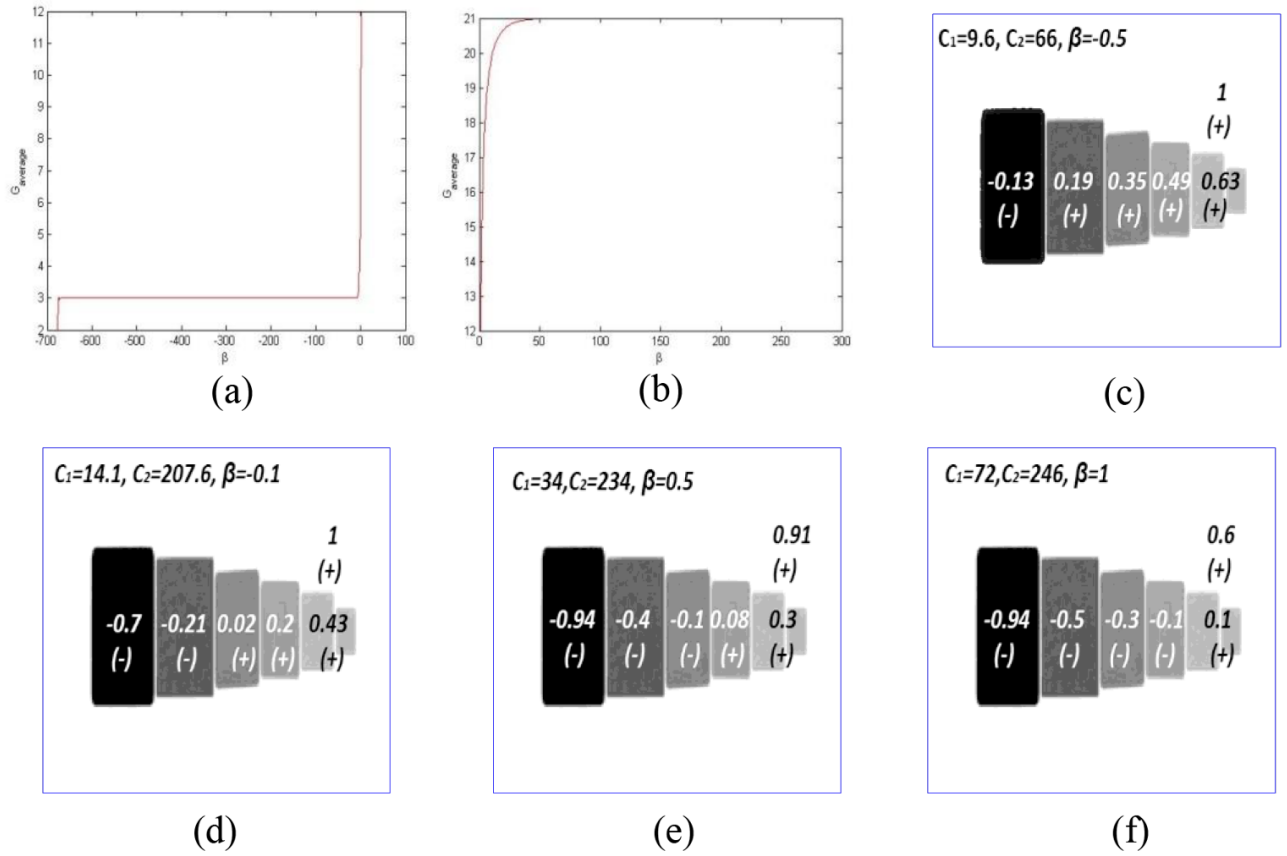

Figure 1. In (a) and (b) numerical overflow is given for $\beta < -679$ and $\beta > 233$ for a set of values $3, 5, \ldots, 21\}$ and $G_{average} \to -\infty, \infty$ respectively. In (c), (d), (e), and (f) signs of the Gspf function inside and outside of the object are given for different values of averages. Clearly the above figures illustrate that a single pair of averages may not help in obtaining the desired result of segmentation. The suitable value of parameter β helps us obtain a suitable pair of averages from the Av-family.

Theorem 2 *Consider an image having q-objects with intensities* $I_1, I_2, \ldots, I_q$, *and let* I_b *be the background intensity. Also let* G_b *and* G_f *be background and foreground averages. Then:*

(I) If $I_1 < I_2 < , \ldots, < I_q < I_b$ (i.e. background intensity is maximum), then for large values of β, $Gspf > 0$ in the background region and $Gspf < 0$ in the foreground.

(II) If $I_b < I_1 < I_2 < \ldots, < I_q$ (i.e. background intensity is minimum), then for large or small β, $Gspf > 0$ in the foreground and $Gspf < 0$ in the background region.

Proof (I) For investigating the sign of $Gspf$ in the background and foreground regions, we proceed as follows:

$$\lim_{\beta\to\infty} Gspf_\beta = \lim_{\beta\to\infty} \frac{I_b - \frac{G_b+G_f}{2}}{\max\left(\left|I_b - \frac{G_b+G_f}{2}\right|\right)} = \frac{I_b - \frac{I_b+I_q}{2}}{\max\left(\left|I_b - \frac{I_b+I_q}{2}\right|\right)} > 0,$$

which means that the sign of the Gspf functions is positive in the background region. □

Next, we consider

$$\lim_{\beta\to\infty} Gspf_\beta = \lim_{\beta\to\infty} \frac{I_q - \frac{G_b+G_f}{2}}{\max\left(\left|I_q - \frac{G_b+G_f}{2}\right|\right)} = \frac{I_q - \frac{I_q+I_b}{2}}{\max\left(\left|I_q - \frac{I_q+I_b}{2}\right|\right)} < 0,$$

which means that the sign of the Gspf functions is negative in the foreground region.

Consequently, the sign of Gspf is negative for objects $I_1<I_2<I_3<,...,<I_{q-1}$. This means that the sign of Gspf is opposite in the background and foreground. Thus, by choosing a suitably large β, all the objects in the image can be detected.

(II) When the background has the minimum intensity and in the foreground we have multiple objects of different intensities, let us have $I_b<I_1<I_2<I_3<,...,<I_q$.

Adopting the same approach, we have:

$$\lim_{\beta\to\infty} Gspf_\beta = \lim_{\beta\to\infty} \frac{I_b - \frac{G_b+G_f}{2}}{\max\left(\left|I_b - \frac{G_b+G_f}{2}\right|\right)} = \frac{I_b - \frac{I_b+I_q}{2}}{\max\left(\left|I_b - \frac{I_b+I_q}{2}\right|\right)} < 0,$$

which means that the sign of the Gspf function is negative in the background region.

Next, we consider

$$\lim_{\beta\to\infty} Gspf_\beta = \lim_{\beta\to\infty} \frac{I_1 - \frac{G_b+G_f}{2}}{\max\left(\left|I_1 - \frac{G_b+G_f}{2}\right|\right)} = \frac{I_1 - \frac{I_q+I_b}{2}}{\max\left(\left|I_1 - \frac{I_q+I_b}{2}\right|\right)} > 0,$$

if $I_1 > \frac{I_q+I_b}{2}$. This means that the sign of the Gspf function is positive in the region with intensity I_1. Thus, in this case the sign of Gspf will be positive in the remaining objects $I_2<I_3<,...,<I_q$ and consequently all the objects in the foreground can be detected. However, if $I_1 < \frac{I_q+I_b}{2}$ then we have an option to choose other suitable values of β for all objects' detection in the foreground because

$$\lim_{\beta\to-\infty} Gspf_\beta = \lim_{\beta\to-\infty} \frac{I_1 - \frac{G_b+G_f}{2}}{\max\left(\left|I_1 - \frac{G_b+G_f}{2}\right|\right)} = \frac{I_1 - \frac{I_b+I_1}{2}}{\max\left(\left|I_1 - \frac{I_b+I_1}{2}\right|\right)} > 0.$$

From Theorem 2 above it can be seen that images with maximum or minimum intensity background can be segmented with this formulation.

Thus, we utilize the Gspf function defined in Eq. (6) in the following manner [10]:

$$\frac{\partial\phi}{\partial t} = \alpha Gspf. \left|\nabla\phi\right|, in\Omega, \quad \text{and } \phi\left(t,x,y\right) = \phi_0\left(x,y\right), in\Omega. \tag{7}$$

The above proposed partial differential equation contains the generalized statistical image intensity information, which derives the contour to the edges that truly represent the objects' boundaries. For numerical solution of Eq. (7) we used an explicit scheme in similar steps as done in [18]. Now we turn our attention towards images having backgrounds of average intensity, which is a challenging case for 2-phase image segmentation models. In the following section we propose a new model to tackle this serious issue.

2.3. Segmenting images of middle-intensity background

Here we propose a new model for segmentation of images having middle-intensity background. For this, let us have an image containing q-objects with the following intensities: $I_1<I_2<I_3<,...,<I_{k-1}<I_k=I_b<I_{k+1}<,...,<I_q$.

Using Eq. (6) we define two functions denoted by G_B and G_F, given by:

$$G_B(u_0) = \frac{u_0(x,y) - \frac{G_{c_1}}{\theta}}{\max\left(\left|u_0(x,y) - \frac{G_{c_1}}{\theta}\right|\right)}, G_F(u) = \frac{u_0(x,y) - \frac{G_{c_2}}{\theta}}{\max\left(\left|u_0(x,y) - \frac{G_{c_2}}{\theta}\right|\right)}, \theta > 0. \tag{8}$$

The function G_B is obtained by putting G_{c_2} equal to zero, and similarly the function G_F is obtained by putting G_{c_1} equal to zero in Eq. (4).

For images whose background is neither of maximum nor minimum intensity, we define a new product spf function, given as:

$$PGspf_{\beta,\theta} = G_B G_F. \tag{9}$$

For segmentation of images we need to have a positive sign of G_B in the background and a negative sign in foreground objects having intensities smaller than I_b, i.e. objects having intensities $I_1, I_2, ..., I_{k-1}$. Similarly, we need to have a negative sign of G_F in the background and a positive sign in foreground objects having intensities smaller than I_b, i.e. objects having intensities $I_1, I_2, ..., I_{k-1}$. This leads the product function $PGspf_{\beta,\theta}$ to have a negative sign in the background and a positive sign in the complete foreground in all the objects. Figure 2 exhibits a middle-intensity background image and explains the idea behind the design of the PGspf function, where the aim is to get the image (PGspf function) where the background and foreground have opposite signs. The given image u as shown in Figure 2 is the image to be segmented. The image u_1 as shown in Figure 2 is the first image obtained by subtracting $\frac{I_q}{\theta}$ from the given image, where I_q denotes the maximum intensity, and for this particular image $\theta \in (1, 2.5)$ is a parameter and in this case we can take 2.1. Next, image u_2 is the image shown in Figure 2 and it can be easily seen that the signs of the background and the foreground are opposite.

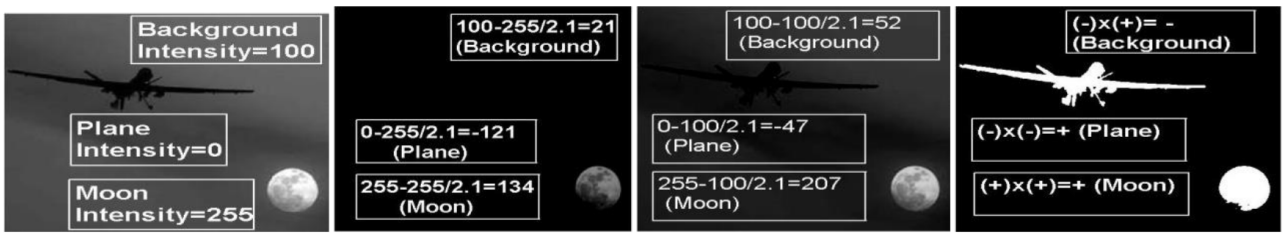

Figure 2. Illustration of the $PGspf_{\beta,\theta}$ function in segmenting a real image having middle-intensity background where maximum intensity (I_q) is 255, background intensity (I_b) is 100, and we choose θ in an interval (1, $\frac{I_q}{I_b} = 2.5$). (a) Given Image u; (b) image $u_1 = u - \frac{I_q}{\theta}$; (c) image $u_2 = u - \frac{I_b}{\theta}$; (d) product image $u_1 \times u_2$, where $\theta = 2.1$.

Now to obtain the desired results from G_B and G_F we establish bounds on parameter θ. Mathematically, we have the following constraints on θ:

$$I_b - \frac{I_b}{\theta} > 0,\ I_q - \frac{I_q}{\theta} > 0,\ I_b - \frac{I_q}{\theta} > 0.$$

From the first two inequalities we get the lower bound $1 < \theta$ and from the third the upper bound $\theta < \frac{I_q}{I_b}$. Thus, the parameter θ exists and its value lies in the interval $1 < \theta < \frac{I_q}{I_b}$.

Thus, based on $PGspf_{\beta,\theta}$ we consider the following evolution problem:

$$\frac{\partial \phi}{\partial t} = \alpha PGspf_{\beta,\theta}. \left|\nabla \phi\right|, \ in\ \Omega, \ \text{where}\, \phi\left(t,x,y\right) = \phi_0\left(x,y\right), \ in\ \Omega. \tag{10}$$

For the numerical solution we use an explicit scheme in similar steps as done in [18].

The overall algorithm can be described in the following steps:

1. Initialize the level set function φ as a binary function.
2. Evolve the level set function φ according to Eq. (7) if an image is either of maximum or minimum intensity background and evolve it according to Eq. (10) if an image is of middle-intensity background (we solve Eqs. (7) and (10) explicitly).
3. Smooth the function φ by Gaussian kernel, i.e. $\varphi = G_\sigma * \varphi$, where σ is the standard deviation.
4. Check whether the evolution is stationary. If not, return to step 2.

For segmentation of color images the above algorithm is applied on each channel (R, G, and B) of the image separately.

In the next section we give some experimental results of the proposed model and some state-of-the-art models.

3. Numerical experiments

In this section, we give experimental results of the proposed generalized signed pressure function-based (GSF) model and compare its results with the state-of-the-art models like the GCV [18], LCV [15], and locally computed spf (LCS) models [1]. From the experimental results it can be seen that our proposed method performs efficiently for images having maximum, minimum, or middle-intensity background.

3.1. Performance of the proposed model for noisy images

In Figure 3, the proposed method is tested on a noisy image. In Figure 3a an original noisy satellite image is given and in Figure 3b the final result of the proposed GSF model is given. Figure 3c displays a multiregion noisy synthetic image and Figure 3d shows the successful detection by the GSF model. We conclude that our proposed model works very well for noisy images. In Figure 4, experimental results of all four models are given on an airplane image.

3.2. Comparison of the four models on images with minimum intensity background

In Figure 5 the proposed model's performance on a saw image having multiple intensity regions and minimum intensity background is compared with LCV, GCV, and LCS. Better performance of our proposed model can be seen in the experimental results and is also verified by JS values.

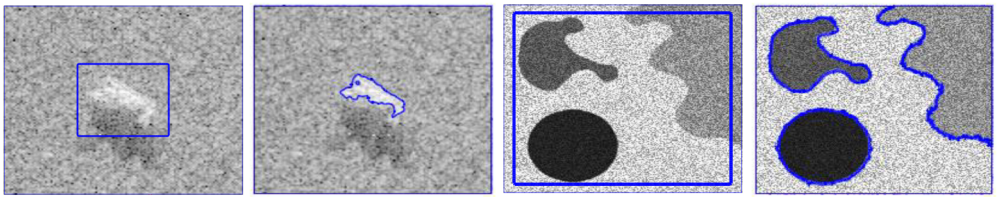

Figure 3. Performance of the GSF model in segmenting real noisy satellite image and a multiregion synthetic noisy image. (a) Real noisy satellite image; (b) result by the GSF model, $\beta = 2$, $\mu = 10$, $iterations = 100$; (c) multiregion synthetic noisy image; (d) result by the GSF model, $\beta = 1.5$, $\mu = 13$, $iterations = 250$, $size(u) = 200 \times 200$.

Figure 4. Experimental test exhibiting that all the four models work well for a simple image: (a) initial guess, (b) GCV result, (c) LCV result, (d) LCS result, (e) GSF result.

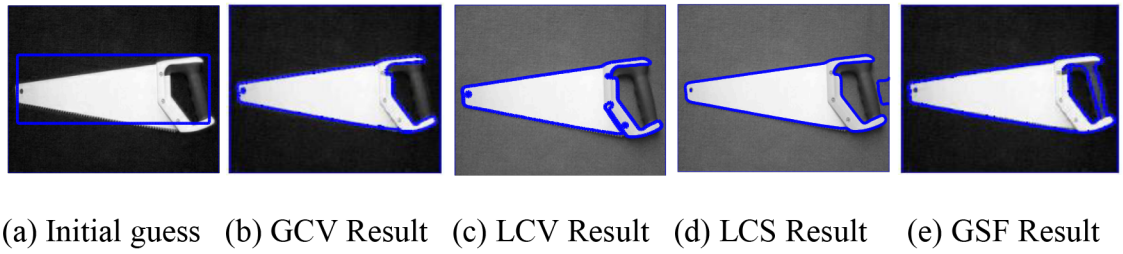

Figure 5. Segmenting a real hardware image having minimum intensity background: (a) initial guess, (b) GCV result, (c) LCV result, (d) LCS result, (e) GSF result. GCV: JS = 0.78, LCV: JS = 0.79, LCS: JS = 0.7, GSF: JS = 0.88. For the proposed model, parameters used are $\beta = -0.906$, $\mu = 77$, $iter = 65$, $size\,(u) = 200 \times 200$.

3.3. Comparison of all models on images with maximum intensity background

In Figure 6, all four models are tested on a real hardware image, which has maximum intensity background and inhomogeneity in its foreground. Our proposed method performs very well for this type of image, while the other methods fail to segment this image. For comparison the JS value for our proposed model is 1.

3.4. Comparison of all models on images with middle-intensity background

The four models are tested on a real multiobject image containing a bird and moon and having middle-intensity background, as given in Figure 7. Our proposed model detected both objects in the image while the other models, the GCV, LCV, and LCS models, could also detect both objects. The JS value for our model is 0.9.

3.5. Selective segmentation results of the proposed model

For selective image segmentation, GCV and GSF are tested on the image given in Figure 8, where the initial contour encloses the kidney to be captured. The GCV model detected the kidney with an undesirable region,

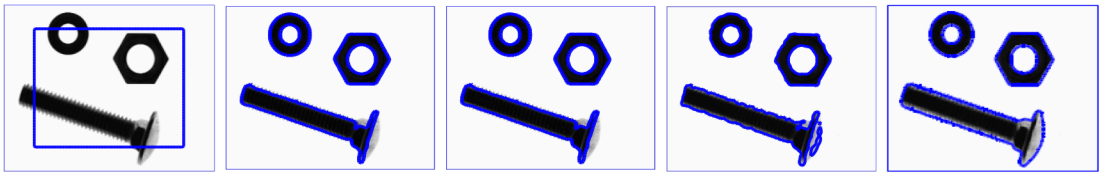

(a) Initial guess (b) GCV Result (c) LCV Result (d) LCS Result (e) GSF Result

Figure 6. Segmenting a real hardware image having maximum intensity background: (a) initial guess, (b) GCV result, (c) LCV result, (d) LCS result, (e) GSF result. GCV: JS = 0.8, LCV: JS = 0.8, LCS: JS = 0.85, GSF: JS = 1. For the proposed model, parameters used are $\beta = 3$, $\mu = 15$, $iter = 100$.

(a) Initial guess (b) GCV Result (c) LCV Result (d) LCS Result (e) GSF Result

Figure 7. Segmenting a real-world image having background intensity neither maximum nor minimum: (a) initial guess, (b) GCV result, (c) LCV result, (d) LCS result, (e) GSF result. GCV: JS = 0.48, LCV: JS = 0.48, LCS: JS = 0.1, GSF: JS = 0.9. For the proposed model, parameters used are $\beta = 3$, $\mu = 40$, $iter = 120$, $\theta = 4$.

whereas the GSF model purely captured the kidney of interest without any undesirable results. Next, it can be easily observed that the proposed GSF model captured the true boundaries of the internal structure of the given brain CT image, whereas the result by the GCV model can also be seen. JS values are given for comparison.

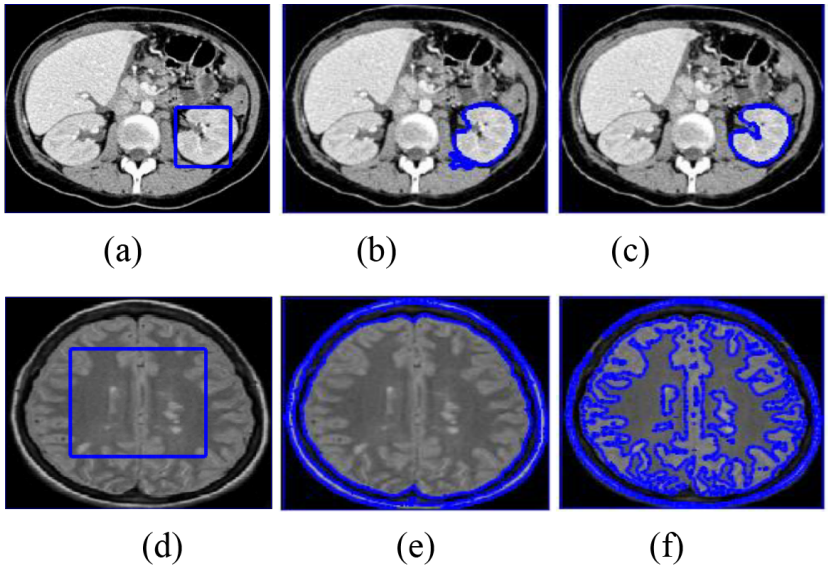

(a) (b) (c)

(d) (e) (f)

Figure 8. Testing the performance of the two models in single and multiple organ segmentation using real medical images: (a) object of interest; (b) GCV result (JS = 0.992); (c) GSF (JS = 0.996); (d) object of interest; (e) GCV result (JS = 0.6); (f) GSF result (JS = 0.8). For GSF the parameters are $\beta = 2$, $\mu = 5(a)$, $\beta = 2$, $\mu = 15$.

3.6. Performance of the GSF model for color images

To exhibit the performance of the proposed model with color images, first, the proposed GSF model and the vector valued Chan–Vese (VVCV) model [5,12] are tested on color images having multiple intensity objects, as in Figure 9. It can be easily observed from these figures that the GSF model successfully captured all the different intensity objects completely in contrast with the standard VVCV model. Similarly, Figure 9 displays an airplane in sky of inhomogeneous intensity. The proposed GSF model successfully detected the airplane in contrast with the VVCV model.

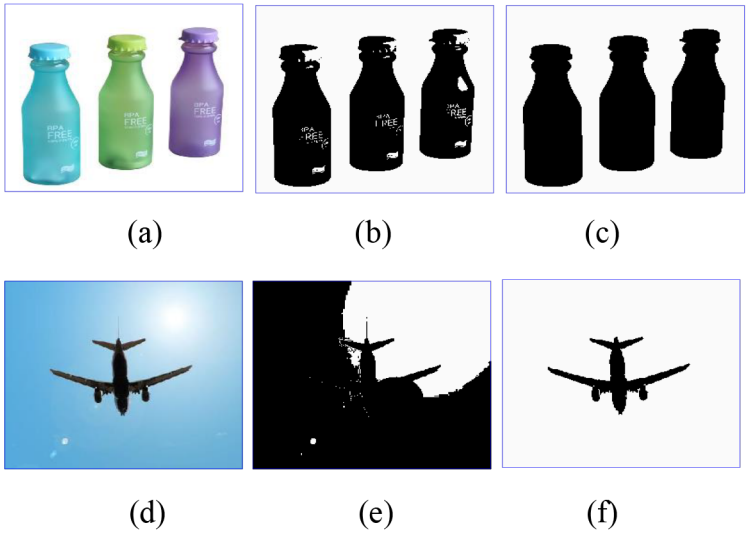

Figure 9. Testing the performance of the GSF and vector valued CV (VVCV) model: for (a) VVCV (JS = 0.81), GSF (JS=0.996), for (d) VVCV (JS=0.5), GSF (JS=0.992). For GSF the parameters used are $\beta = 5$, $\mu = 20$, $iter = 100$ for (a) and $\beta = 0.5$, $\mu = 10$, $iter = 100$ for (d).

3.7. Speed comparison of all four models

Next, using the image in Figure 3a, the time comparisons of all four models are given in Table 1. These experiments were done using MATLAB 7.11.0, with Windows 7 and a 2.53 GHz Intel Core i3 personal computer with 2 GB RAM. The following notations are used in Table 1: Size, the size of given image $m \times n$; Iter, the total number of iterations; CPU, the CPU time in seconds. From the table it can be seen that our model is as fast as GCV, because in both models we are solving the same partial differential equation, but we are using different spf functions. LCV is fast in time but its performance is limited in the above discussed problems. In Table 2, a quantitative comparison of different models in terms of the mean $\pm$ SD of JS values is given, where SD is the

Table 1. CPU time comparison of the LCV, GCV, LCS, and our proposed GSF model.

Size	GSF		GCV method		LCV method		LCS method	
	Iter	CPU	Iter	CPU	Iter	CPU	Iter	CPU
200 ×200	17	0.4	17	0.4	2	0.3	62	3.4
400 ×400	50	3	50	3	2	0.7	166	36
600 ×600	80	17	80	17	2	2	290	208
800 ×800	110	31	110	31	2	2.6	430	498

Table 2. Mean and SD of JS values for state-of-the-art models tested on images with different background intensities.

Intensity	GCV model	LCV model	LCS model	GSF model
Maximum	0.68 ± 0.1	0.6 ± 0.1	0.88 ± 0.03	0.98 ± 0.02
Minimum	0.73 ± 0.04	0.8 ± 0.11	0.8 ± 0.1	0.96 ± 0.02
Middle	0.57 ± 0.2	0.53 ± 0.2	0.5 ± 0.3	0.93 ± 0.03

standard deviation. For JS value comparisons we have used synthetic images with maximum, minimum, and middle-intensity backgrounds like the images given in Figures 1, 2, 5, 6, and 7. It can be observed that our proposed model gives better JS values for different problems.

4. Conclusion

In this paper we have proposed a novel active contour model based on generalized averages and spf functions for segmenting images that have multiple objects, having either maximum, minimum, or middle-intensity backgrounds. For images with constant intensities, all four state-of-the-art models work well, but images having multiple regions can only be segmented by our proposed GSF model, which can be seen from the experiments. However, images in which objects have intensity inhomogeneity may not be segmented efficiently by the proposed algorithm, which is our future task.

References

[1] Akram F, Kim J, Lim H, Choi K. Segmentation of intensity inhomogeneous brain MR images using active contours. Comput Math Method M 2014; 2014: 194614.

[2] Ali H, Badshah N, Chen K, Khan GA. A variational model with hybrid images data fitting energies for segmentation of images with intensity inhomogeneity. Pattern Recogn 2016; 51: 27-42.

[3] Badshah N, Chen K, Ali H, Murtaza G. Coefficient of variation based image selective segmentation using active contour. East Asian J Appl Math 2012; 2: 150-169.

[4] Caselles V, Kimmel R, Sapiro G. Geodesic active contours. Int J Comput Vision 1997; 22: 61-79.

[5] Chan T, Vese L. Active contours without edges. IEEE T Image Process 2001; 10: 266-277.

[6] Chen K. Matrix Preconditioning Techniques and Applications. 1st ed. Cambridge UK: Cambridge University Press, 2005.

[7] Guyader C, Gout C. Geodesic active contour under geometrical conditions theory and 3D applications. Numer Algorithms 2008; 48: 105-133.

[8] Kass M, Witkin A, Terzopoulos D. Active contours models. Int J Comput Vision 1988; 1: 321-331.

[9] Li C, Kao C, Gore J, Ding Z. Implicit active contours driven by local binary fitting energy. In: Proceedings of the IEEE Conference on Computer Vision and Pattern Recognition; 2007. New York, NY, USA: IEEE. pp. 1-7.

[10] Mumford D, Shah J. Optimal approximation by piecewise smooth functions and associated variational problems. Commun Pure Appl Math 1989; 42: 577-685.

[11] Murtaza G, Ali H, Badshah N. A robust local model for segmentation based on coefficient of variation. J Inf Commun Technol 2011; 5: 30-39.

[12] Osher S, Fedkiw R. Γ-Level set methods and dynamic implicit surfaces. Lect Notes Comp Sci 2005; 3708: 499-506.

[13] Chan TF, Sandberg BY, Vese LA. Active contour without edges for vector valued images. J Vis Commun Image R 2000; 11: 130-140.

[14] Vese LA, Chan TF. A multiphase level set framework for image segmentation using the Mumford and Shah model. Int J Comput Vision 2002; 50: 271-293.

[15] Wang X, Huang D, Xu H. An efficient local Chan-Vese model for image segmentation. Pattern Recogn 2010; 43: 603-618.

[16] Zhang K, Song H, Zhang L. Active contours driven by local image fitting energy. Pattern Recogn 2010; 43: 1199-1206.

[17] Zhang C, Zhang Y, Lin Z. Automatic face segmentation based on the level set method. In: National Conference on Information Technology and Computer Science; 16–18 November 2012; Lanzhou, China. pp. 678-681.

[18] Zhang K, Zhang L, Song H, Zhou W. Active contours with selective local or global segmentation: a new formulation and level set method. Imag Vision Comput 2010; 28: 668-676.